JOURNAL OF COMPUTATIONAL PHYSICS 83, 463–484 (1989)

Chebyshev Pseudospectral Solution of the Stokes Equations Using Finite Element Preconditioning

P. DEMARET AND M. O. DEVILLE

Université Catholique de Louvain, Unité de Mécanique Appliquée, Louvain-La-Neuve, Belgium

Received November 4, 1987; revised October 11, 1988

The Stokes equations are solved by a Chebyshev pseudospectral method on a rectangular domain. As the resulting system of algebraic equations is very difficult to factorize, a preconditioning is designed using a finite element technique. The fem solver constitutes the masterpiece of a Richardson iteration process. Several finite elements are investigated: the 9-nodes Lagrangian element $Q2$–$Q1$, the $Q1$–$Q0$ element, and the $Q1$–$Q1$ element due to Brezzi and Pitkaranta. An eigenvalue analysis is carried out in order to pinpoint the characteristic features of each preconditioner. It is shown that the $Q2$–$Q1$ element yields the best convergence results. The power of this choice is demonstrated on theoretical solutions and on the regularized square cavity problem.

1. INTRODUCTION

This paper deals with the numerical integration of the linear Stokes equations using Chebyshev approximations for the primitive variables (velocity–pressure formulation). Among the various spectral projection methods available to the numericists [1, 2], the pseudospectral technique constitutes at the present time the best choice to cope with nonconstant coefficients in the partial differential equations or with complex geometries, while still retaining spectral accuracy ("infinite order" of convergence for smooth problems).

As usual, the major bottleneck of the pseudospectral calculation comes from the solution of the linear system, as resulting matrices are not banded and not very well conditioned. Therefore, in order to reduce the computational intensive work needed to produce the answer, preconditioning algorithms are designed. S. A. Orszag [3] and Y. Morchoisne [4] proposed independently to work with finite difference (FD) preconditioning. Haldenwang *et al.* [5] showed for the Helmholtz equation that this preconditioning converges if the iterative method is underrelaxed. This conclusion contrasts greatly with the results obtained by Deville and Mund [6] with finite element preconditioning for general second-order elliptic equations, where no underrelaxation was applied. This better behaviour may be explained by an eigenvalue analysis of the preconditioned pseudospectral operator [7] and allows in some cases to even practise overrelaxation.

0021-9991/89 $3.00

This good performance together with the ability of treating complicated geometries through the finite element (FE) method convinced us to investigate FE preconditioning of Chebyshev pseudospectral solutions of the Stokes equations. Preliminary results were already showed at the Ninth International Conference on Numerical Methods Fluid Dynamics [8]. Of course, it is very worthwhile and time-saving to resort to existing codes as preconditioners. In some sense, the strategy is the same as in car racing where the turbo part coming on top of a conventional atmosphere engine provides power and milecrunching. In the numerical world, Chebyshev methods yield the computational power and the FE code offers a well-known and performing tool for number-crunching.

Section 2 presents the basic equations, set definitions, and notations and describes the pseudospectral approximation. Section 3 introduces briefly each finite element preconditioner and, in particular, carries out an eigenvalue analysis of the preconditioned pseudospectral operator. This analysis will allow us to discuss the pros and cons for each preconditioner. Section 4 deals with numerical results on analytical solutions and a test problem. The last section draws the conclusions of this investigation.

2. Basic Equations and Algorithms

2.1. *Basic Equations*

The stationary Stokes equations express, that for a zero Reynolds number, the momentum equations are for a Newtonian fluid

$$\sigma_{ji,j} + \rho f_i = 0, \tag{2.1a}$$

$$\sigma_{ij} = -p\delta_{ij} + 2\mu d_{ij}, \tag{2.1b}$$

$$d_{ij} = \tfrac{1}{2}(u_{i,j} + u_{j,i}), \tag{2.1c}$$

where u_i denote the components of the velocity field, p the pressure, μ the dynamic viscosity, and f_i the components of the external forces. The components of the stress tensor σ_{ij} depend linearly on the components d_{ij} of the rate of deformation tensor through (2.1b). As the fluid will be assumed incompressible, the flow must satisfy the continuity constraint

$$u_{i,i} = 0. \tag{2.2}$$

Summation over repeated indices is assumed. The comma notation means partial differentiation. Equations (2.1) and (2.2) are solved on the domain Ω. The boundary conditions will be formally expressed as

$$B\bar{u} = \bar{g}, \qquad \text{on } \partial\Omega, \tag{2.3}$$

where the bar is used for vector notation.

The boundary condition operator B splits in two parts. The first one applies the essential conditions on $\partial\Omega_e$, i.e.,

$$\bar{u}(\bar{r}) = \bar{g}_1(\bar{r}), \qquad \forall \bar{r} \in \partial\Omega_e. \tag{2.4}$$

In (2.4), $\bar{r}$ denotes the position vector of a point. The second part of the boundary is concerned with natural conditions:

$$\bar{t}(\bar{r}) = \bar{\bar{\sigma}} \cdot \bar{n} = \bar{g}_2(\bar{r}), \qquad \forall \bar{r} \in \partial\Omega_n, \tag{2.5}$$

where $\bar{\bar{\sigma}}$ is the stress tensor defined by (2.1b) and $\bar{n}$ the unit outward normal vector to that part of $\partial\Omega$.

This linear set of equations will be solved by the Chebyshev pseudospectral approximation method.

2.2. *Notations and Definitions*

In this paper, we borrow and extend the notations from Canuto and Pietra [9]. Let us denote by N the couple $(N_{X1}, N_{X2}) \in \mathbf{N} \times \mathbf{N}$, where $\mathbf{N}$ is the set of natural numbers (positive integers). The discrete Chebyshev mesh $\mathbf{G}_N$ results from the tensor product of 1-dimensional Gauss–Lobatto–Chebyshev (GLC) quadrature grids,

$$\mathbf{G}_N = \bigotimes G_{xi, Nxi}, \qquad i = 1, 2, \tag{2.6}$$

with $G_{xi, Nxi}$ being the roots of the equation

$$(1 - x^2)\, T'_{Nxi} = 0, \qquad x \in [-1, 1], \tag{2.7}$$

In this relation, T_{Nxi} is the Chebyshev polynomial of first kind and degree N_{xi}. Therefore, the GLC grid contains the points:

$$x_k = \cos \frac{\pi k}{N_{xi}}, \qquad k = 0, \ldots, N_{xi}. \tag{2.8}$$

Let R_N represent the collection of rectangles whose vertices are four neighbouring gridpoints of $\mathbf{G}_N$ such that $R_N = \bigcup_i R_i$. Let $\mathbf{P}_{(n,n)}$ denote the space of 2-rectangles of type (n) or 2-dimensional Lagrangian finite elements which restrict to a nth degree polynomial over each rectangle $R_i \in R_N$. Here we will consider $n = 0$, 1, or 2 [10].

The space $\mathbf{P}_N$ will contain all the continuous functions in $\bar{\Omega} = \Omega \cup \partial\Omega$, which are Chebyshev orthogonal polynomials of degree N_{xi} in the x_i variable.

As the Chebyshev pseudospectral scheme will be preconditioned by finite elements, we have to define a few spaces related to this method. The velocities will come from $V_{n,h}$:

$$V_{n,h} = \{v_h \in C^0(\bar{\Omega}) \mid \forall R_i \in R_N,\ v_{h|R_i} \in \mathbf{P}_{(n,n)},\ n = 1, 2\}, \tag{2.9}$$

while the pressure belongs to $P_{n,h}$:

$$P_{n,h} = \{q_h \in L^2(\bar{\Omega}) \,|\, \forall R_i \in R_N,\ q_{h|R_i} \in \mathbf{P}_{(n,n)},\ n = 0, 1\}. \tag{2.10}$$

Given a smooth continuous function φ on $\partial\Omega$, $V_{n,h}(\varphi)$ will be the affine space of the functions in $V_{n,h}$ which coincide with φ at the boundary nodes of $\partial\Omega_e$:

$$V_{n,h}(\varphi) = \{v_h \in V_{n,h} \,|\, v_h(\bar{r}_b) = \varphi(\bar{r}_b),\ \forall \bar{r}_b \in \mathbf{G}_{n,N} \cap \partial\Omega_e\}. \tag{2.11}$$

An interesting particular case is the subspace $V_{n,h}(0)$ which will be denoted in short by:

$$V^0_{n,h} = V_{n,h}(0).$$

In (2.11), the grid $\mathbf{G}_{n,N}$ is the set of global nodes for the (N_{X1}, N_{X2}) FE mesh in Ω with 2-rectangle of type (n), $n = 0, 1, 2$. For $n = 1$, notice that $\mathbf{G}_N \equiv \mathbf{G}_{1,N}$. The $\mathbf{G}_{0,N}$ grid is built up with the nodal values attached to the centroid of R_i. Associated with these partitions, one has a set of linear functionals $l_{\mathbf{G}_{n,N}}$ defined on the global grid $\mathbf{G}_{n,N}$. At the elemental level (or local grid), this set corresponds to a nth degree bivariate Lagrange interpolation problem. It is clear that $l_{\mathbf{G}_{n,N}}$ is an isomorphism of the set of nodal values defined on $\mathbf{G}_{n,N}$.

Let us now define some important interpolation operators pertinent for the preconditioning technique. The notation I_h will represent the finite element interpolator on the Lagrangian basis functions:

$$I_h^{n,m} = \begin{cases} I^v_{n,h}: C^0(\bar{\Omega}) \to V_{n,h} \\ (I^v_{n,h} v)(\bar{r}_i) = l_{\mathbf{G}_{n,N}} v(\bar{r}_i), & \forall \bar{r}_i \in \mathbf{G}_{n,N} \\ I^q_{m,h}: \begin{Bmatrix} C^0(\bar{\Omega}) \\ \text{or} \\ L^2(\bar{\Omega}) \end{Bmatrix} \to P_{m,h} \\ (I^q_{m,h} q)(\bar{r}_i) = l_{\mathbf{G}_{m,N}} q(\bar{r}_i), & \forall \bar{r}_i \in \mathbf{G}_{m,N}. \end{cases} \tag{2.12}$$

A particular case arises when velocities satisfy homogeneous Dirichlet conditions. Denoting this case by I^0_h, one obtains

$$I_h^0 = \begin{cases} I^v_{n,h}: C^0(\bar{\Omega}) \to V^0_{n,h} \\ (I^v_{n,h} v)(\bar{r}_i) = \begin{cases} l_{\mathbf{G}_{n,N}} v(\bar{r}_i), & \forall \bar{r}_i \in \mathbf{G}_{n,N} \cap (\bar{\Omega} \backslash \partial\Omega_e) \\ 0, & \forall \bar{r}_i \in \mathbf{G}_{n,N} \cap \partial\Omega_e \end{cases} \\ I^q_{m,h}: \begin{Bmatrix} C^0(\bar{\Omega}) \\ \text{or} \\ L^2(\bar{\Omega}) \end{Bmatrix} \to P_{m,h} \\ (I^q_{m,h} q)(\bar{r}_i) = l_{\mathbf{G}_{m,N}} q(\bar{r}_i), & \forall \bar{r}_i \in \mathbf{G}_{m,N}. \end{cases} \tag{2.13}$$

Of course, we need a spectral interpolation operator acting from a discrete set of values into $\mathbf{P}_N$. The spectral interpolation for the velocities is defined as

$$I_N^v = \begin{cases} I_N^v : C^0(\bar{\Omega}) \to \mathbf{P}_N \\ (I_N^v v)(\bar{r}_i) = v(\bar{r}_i), \qquad \forall \bar{r}_i \in \mathbf{G}_N. \end{cases} \tag{2.14}$$

For the pressure, we will distinguish two cases. The first one is described by the relations

$$I_N^{q,1} = \begin{cases} I_N^{q,1} : C^0(\bar{\Omega}) \to \mathbf{P}_N \\ (I_N^{q,1} q)(\bar{r}_i) = q(\bar{r}_i), \qquad \forall \bar{r}_i \in \mathbf{G}_N, \end{cases} \tag{2.15}$$

while the second case corresponds to the next equations:

$$I_{N-1}^{q,0} = \begin{cases} I_{N-1}^{q,0} : L^2(\bar{\Omega}) \to \mathbf{P}_{N-1} \\ (I_{N-1}^{q,0} q)(\bar{r}_i) = q(\bar{r}_i), \qquad \forall \bar{r}_i \in \mathbf{G}_{0,N}. \end{cases} \tag{2.16}$$

The pressure computed on the $\mathbf{G}_{0,N}$ grid will be filtered to get rid of the spurious checkerboard (CB) mode. To this end, one introduces the restriction operator R_{N-1} such that

$$R_{N-1} = \begin{cases} R_{N-1} : \mathbf{P}_{N-1} \to \mathbf{P}_{N-2} \\ (R_{N-1} I_{N-1}^{q,0} q)(\bar{r}_i) = q(\bar{s}_i), \qquad \forall \bar{r}_i \in \mathbf{G}_{0,N}, \ \forall \bar{s}_i \in \mathbf{G}_{0,CB}. \end{cases} \tag{2.17}$$

In (2.17), the new mesh $\mathbf{G}_{0,CB}$ is defined by the next relationship

$$\mathbf{G}_{0,CB} = \left\{ (x_i, y_j) \,|\, x_i = \frac{1}{2}\left(\cos\frac{2i-1}{N_{x1}} \cdot \frac{\pi}{2} + \cos\frac{2i+1}{N_{x1}} \cdot \frac{\pi}{2} \right), \ i = 1 \ldots N_{x1}, \right.$$
$$\left. y_j = \frac{1}{2}\left(\cos\frac{2j-1}{N_{x2}} \cdot \frac{\pi}{2} + \cos\frac{2j+1}{N_{x2}} \cdot \frac{\pi}{2} \right), \ j = 1 \ldots N_{x2} \right\}. \tag{2.18}$$

Note that this grid contains only $(N-1)^2$ discrete points if $N_{x1} = N_{x2} = N$.

The full spectral interpolator which encompasses velocities and pressure will be written as I_N with the meaning:

$$I_N = \begin{cases} I_N^v, & I_N^v \\ & \text{or} \\ I_N^{q,1}, & R_{N-1} I_{N-1}^{q,0}. \end{cases} \tag{2.19}$$

The context of the usage of (2.19) will make clear which definition is in application.

2.3. *Pseudospectral Approximation*

The pseudospectral approximation is a weighted residual method where the residual is evaluated by insertion of the finite development of the dependent

variables with respect to basis functions $\varphi_i(\bar{r})$. Denoting by u_N a typical dependent variable, one gets

$$u_N = \sum_{i=0}^{N_{x1}} \sum_{j=0}^{N_{x2}} u_{ij} \varphi_i(x_1)\, \varphi_j(x_2), \tag{2.20}$$

where

$$\begin{aligned} \varphi_i(z) &= \frac{(1-z^2)\, T'_{Nz}(z)(-1)^{i+1}}{\bar{c}_i N_z^2 (z - z_i)}, \qquad i = 0, ..., N_z, \\ \bar{c}_0 &= \bar{c}_{Nz} = 2; \qquad \bar{c}_i = 1, \qquad i = 1, ..., N_z - 1. \end{aligned} \tag{2.21}$$

The functions defined in (2.21) satisfy

$$\varphi_i(z_k) = \delta_{ik}.$$

Then, the projection method requires that the scalar product (usually defined by a quadrature) of the residual with well-chosen weight functions vanishes. For the pseudospectral scheme, these weight functions are Dirac distributions. The partial differential problem is required to be solved *exactly* on a discrete set of interior collocation points while the boundary conditions are enforced on $\partial\Omega$. This collocation procedure depends very much on the choice of collocation nodes. Here, these nodes are the zeroes associated with the Gauss–Lobatto–Chebyshev quadrature rule.

The pseudospectral equations are gotten combining (2.1a) and (2.1b):

$$\left.\begin{aligned} (-\operatorname{grad} p + 2\mu \operatorname{div} \bar{\bar{d}} + \rho \bar{f})(\bar{r}_i) &= 0, \\ (\operatorname{div} \bar{u})(\bar{r}_i) &= 0, \end{aligned}\right\} \forall \bar{r}_i \in \mathbf{G}_N \cap \Omega,$$
$$\bar{u}(\bar{r}_i) = \bar{g}_1(\bar{r}_i), \qquad \forall \bar{r}_i \in \mathbf{G}_N \cap \partial\Omega_e, \tag{2.22}$$
$$\bar{\bar{\sigma}} \cdot \bar{n}(\bar{r}_i) = \bar{g}_2(\bar{r}_i), \qquad \forall \bar{r}_i \in \mathbf{G}_N \cap \partial\Omega_n.$$

If L^{st} denotes the Stokes differential operator corresponding to the two first equations of (2.22), the matrix system equivalent to (2.22) may be cast in the form

$$L_{\mathrm{ps}} \bar{x} = \bar{b}, \tag{2.23}$$

where

$$\begin{aligned} L_{\mathrm{ps}} &= \begin{bmatrix} L^{\mathrm{st}}_{\mathrm{ps}} \\ B_{\mathrm{ps}} \end{bmatrix}, \qquad \bar{x} = \begin{bmatrix} \bar{u} \\ p \end{bmatrix}, \\ \bar{b} &= \begin{bmatrix} \bar{b}^{\mathrm{st}} \\ \bar{b}^{\mathrm{bc}} \end{bmatrix}, \qquad \bar{b}^{\mathrm{st}} = \begin{bmatrix} -\rho \bar{f} \\ 0 \end{bmatrix}, \qquad \bar{b}^{\mathrm{bc}} = \begin{bmatrix} \bar{g}_1 \\ \bar{g}_2 \end{bmatrix}. \end{aligned} \tag{2.24}$$

Instead of solving (2.23), the pseudospectral system is preconditioned in order to

reduce the condition number of the algebraic system and to take ample profit of well-known and efficient solvers. The preconditioned Richardson iteration consists in the next relationship

$$\bar{x}^{(k+1)} = \bar{x}^{(k)} - \alpha_k \hat{L}^{-1}(L_{ps}\bar{x}^{(k)} - \bar{b}), \tag{2.25}$$

where

$$\hat{L} = L_{FE} \tag{2.26}$$

is the approximate operator based on a finite element approach. In (2.25), the superscript is an iteration counter.

If the sequence of iterates $\bar{x}^{(k)}$ converges, Eq. (2.25) leads to the solution of (2.23). The initial guess for (2.25) comes from

$$\bar{x}^{(0)} = I_N \bar{w}_h, \tag{2.27}$$

where $\bar{w}_h$ is the solution of the finite element problem

$$\begin{gathered} 2\mu \int_\Omega \bar{\bar{d}}_h \operatorname{grad} \bar{v}_h \, d\Omega - \int_\Omega p_h \operatorname{div} \bar{v}_h \, d\Omega = \int_\Omega \rho \bar{f} \bar{v}_h \, d\Omega + \int_{\partial\Omega_n} \bar{g}_2 \bar{v}_h \, dl, \\ \int_\Omega q_h \operatorname{div} \bar{u}_h \, d\Omega = 0, \qquad \bar{f}, \bar{g}_2 \in L^2(\bar{\Omega}), \\ \bar{w}_h = \begin{bmatrix} \bar{u}_h \\ p_h \end{bmatrix}. \end{gathered} \tag{2.28}$$

In (2.28), the components of $\bar{v}_h$ and q_h belong to $V_{n,h}$ and $P_{n,h}$, respectively. This will be discussed in more detail in the next section. The subsequent iterations are defined by the equation

$$\bar{x}^{(k+1)} = \bar{x}^{(k)} - \alpha_k I_N L_{FE}^{-1}[I_h^{n,m}(L_{ps}\bar{x}^{(k)} - \bar{b}), J_h^{n,m}(\bar{\bar{\sigma}}^{(k)} \cdot \bar{n} - \bar{g}_2)], \tag{2.29}$$

where the relaxation parameter α_k plays an essential role. Its choice will depend on the eigenvalue spectrum of $L_{FE}^{-1} L_{ps}$. In (2.29), one introduces $J_h^{n,m}$ a finite element interpolator on the portion of the boundary where natural boundary conditions are prescribed. The definition of $J_h^{n,m}$ is

$$J_h^{n,m}(\bar{t}) = \begin{cases} (I_{n,h}^v v)(\bar{r}_i) = \boldsymbol{l}_{G_{n,N}} v(\bar{r}_i), & \forall \bar{r}_i \in \mathbf{G}_{n,N} \cap \partial\Omega_n, \\ 0, & \forall \bar{r}_i \in \mathbf{G}_{n,N} \cap \partial\Omega_e, \\ (I_{m,h}^q q)(\bar{r}_i) = \boldsymbol{l}_{G_{m,N}} q(\bar{r}_i), & \forall \bar{r}_i \in \mathbf{G}_{m,N} \cap \partial\Omega_n, \\ 0, & \forall \bar{r}_i \in \mathbf{G}_{m,N} \cap \partial\Omega_e. \end{cases} \tag{2.30}$$

At a point where $\partial\Omega_n$ and $\partial\Omega_e$ intersect, the essential condition is enforced. For readers more familiar with a matrix formulation, Eq. (2.29) may be written as

$$\bar{x}^{(k+1)} = \bar{x}^{(k)} - \alpha_k K^{-1} M R^{(k)}, \tag{2.31}$$

where K is the stiffness matrix and M the mass matric of the finite element approximation. The notation $R^{(k)}$ defines the quantities

$$R^{(k)} = \begin{bmatrix} L_{ps}^{st}\bar{x}^{(k)} - \bar{b}^{st} \\ 0 \\ \bar{\bar{\sigma}} \cdot \bar{n} - \bar{g}_2 \end{bmatrix} \tag{2.32}$$

Returning to (2.28) and (2.29), the integrals involved in these expressions are calculated at the elemental level by a Gauss–Legendre (GL) quadrature rule with three points in each space direction. The various spectral interpolators I_N (2.14)–(2.16) yield the needed values at the nodes of the GL rule. The residue calculation (2.32) on the $\mathbf{G}_N$ grid may be performed in two ways. The first one resorts to matrix multiplications to carry out derivative operations. This is extremely efficacious on a vector computer because of the high vectorization level achieved by most systems on matrix computations. The second track uses a FFT algorithm with possible pre- and post-processings to take all the symmetries into account. The residual evaluation is done in Chebyshev space by recurrence equations and real values are restored through inverse discrete Chebychev transforms (DCT [11]). This scheme is more efficient on serial machines as it operates in $O(N.\log(N))$ floating point operations per second (flops) compared to N^2 flops for matrix multiplications. For other points such that $r_i \in \mathbf{G}_{n,N} \backslash \mathbf{G}_N$, the values are obtained by Clenshaw recurrence.

Once the computation is ended at the elemental level, the full matrix system is built up by direct stiffness and solved by LU factorization for sparse matrices with minimum-degree ordering [12, 13].

We should stress at this point that the previous procedure of residual calculation at the GL nodes differs from the classical collocation methods. We might call it *pseudocollocation* after a suggestion by C. Canuto. However, it offers the advantage of taking full power of finite element know-how as it can be easily extended to general geometries with isoparametric transformations generating geometric coefficients inside the quadrature rule.

The convergence of the preconditioned pseudospectral iterative process depends on the spectral radius of $I - A$, where $A = K^{-1}ML_{ps}$, and therefore on the condition number of A. We will consider $\kappa(A) = \lambda_{max}/\lambda_{min}$ as a measure of the condition number of A even when A is not symmetric, λ_{max} and λ_{min} being the maximum and minimum eigenvalues of A, respectively. These eigenvalues are given by their modulus.

3. Finite Element Preconditioners

The finite element approximation of fluid flow computations requires the imposition of an inf-sup stability condition due to Brezzi and Babuska [14, 15], which provides compatibility between computed pressure and velocities in order to avoid

TABLE I

Minimum and Maximum Eigenvalue of the Pseudospectral Stokes Problem with Respect to the Chebyshev Cutoff Value

N	λ_{max}	λ_{min}
5	−58.43	−0.0797
7	−223.84	−0.0359
9	−646.73	−0.0205
11	−1528.74	−0.0131
13	−3124.22	−0.0090

the presence of spurious oscillating pressure modes. Three types of velocity–pressure elements are investigated in the present paper:

(I) the $Q2$–$Q1$ element (biquadratic velocities; bilinear pressures);

(II) the $Q1$–$Q1$ element proposed by Brezzi and Pitkaranta [16];

(III) the $Q1$–$Q0$ element (bilinear velocities; constant pressures).

The element I satisfies the Babuska–Brezzi condition while element III fails the test. Element II solves a perturbed problem which does not call for such a condition. The choice of I is motivated by the fact that the element vertices coincide with $\mathbf{G}_N$. However, this element induces a large amount of computer time as the velocities belong to $V_{2,h}$, thereby increasing the bandwidth of the matrix system. Element II seems to be a better choice from the computational point of view because velocities and pressures are in $V_{1,h}$ and $P_{1,h}$, respectively. Finally, element III implements a staggered approach and offers a reduced computing time with velocities and pressure in $V_{1,h}$ and $P_{0,h}$, respectively. This element is the finite element counterpart of a collocation technique designed for the Navier–Stokes

TABLE II

Condition Number of A for the Stokes Problem Preconditioned by $Q2$–$Q1$ Finite Elements. Dirichlet Boundary Conditions

N	λ_{max}	λ_{min}	$\frac{\lambda_{max}}{\lambda_{min}} = \kappa(A)$
5	1.916	1.9943	1.927
7	1.926	0.9974	1.931
9	1.913	0.9963	1.920
11	1.993	0.9933	2.006
13	2.007	0.9899	2.003
15	2.008	0.9865	2.036

equations by Malik *et al.* [17]. The pseudospectral method was preconditioned by finite differences on a staggered grid.

From the spectral side, we have to recall that in the 2D case, the velocity–pressure formulation with the Chebyshev approximation has spurious pressure modes when velocities and pressure are attached to the same nodes of $\mathbf{G}_N$. This phenomenon was first noticed by Morchoisne [18], and Bernardi *et al.* [19] proved that the dimension of the subspace containing all spurious pressure modes is equal to 8.

Now, we proceed to a careful examination of each preconditioner.

3.1. *The Q2–Q1 Element*

Here, the preconditioned pseudospectral iteration algorithm becomes

$$\bar{x}^{(k+1)} = \bar{x}^{(k)} - \alpha_k I_N L_{\mathrm{FE}}^{-1} [I_h^{2,1}(L_{\mathrm{ps}}\bar{x}^{(k)} - \bar{b}),\, J_h^{2,1}(\bar{\bar{\sigma}}^{(k)} \cdot \bar{n} - \bar{g}_2)]. \tag{3.1}$$

The eigenvalue analysis of $A = L_{\mathrm{FE}}^{-1} I_h^{2,1} L_{\mathrm{ps}}$ was carried out. For the sake of simplicity, let us take $N_{xi} = N$. Table I reports the numerical results of the extreme eigenvalues of $L_{\mathrm{ps}}^{\mathrm{st}}$ with respect to an increase of the number of degrees of freedom. Notice that the maximum eigenvalue behaves like a function of N^4. This result is not surprising as the Stokes problem is a second-order elliptic problem. Each eigen-

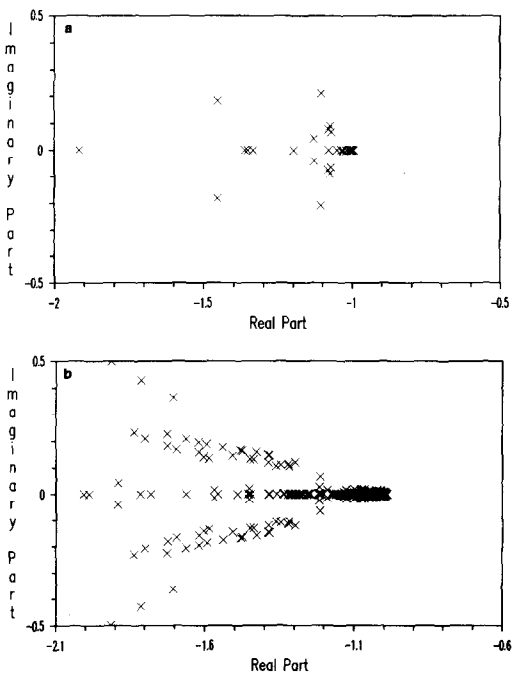

FIG. 1. Eigenvalue spectrum of A. Stokes problem preconditioned by $Q2$–$Q1$ FE. Dirichlet boundary conditions: (a) $N = 5$, (b) $N = 13$.

value analysis yields seven zero eigenvalues corresponding to the spurious pressure modes, as the hydrostatic mode is removed by imposing a reference pressure. Therefore, the first minimum nonvanishing eigenvalue decreases like $N^{-2.3}$ with finer discretization. In Table II the condition number of A is examined for a Stokes flow with Dirichlet boundary conditions. For higher N values, it is close to 2. This behaviour emphasizes the quality of this preconditioner. The optimal value of α_k is $\frac{2}{3}$. Figures 1a and b display the clustering of the spectrum of A between -1 and -2 with $N=5$ and 13.

In Table III, the condition number of A is analyzed for a Stokes flow where $\partial\Omega_n = \{x=1;\ y=1\}$. The minimum eigenvalue goes to unity with increasing d.o.f., while $\lambda_{\max}$ gets close to $\pi^2/4$. Figures 2a and b show the eigenvalue spectrum which has broadened with respect to the Dirichlet case, for $N=5$ and 13.

3.2. *The Q1–Q1 Element*

The iterative algorithm is

$$\bar{x}^{(k+1)} = \bar{x}^{(k)} - \alpha_k I_N L_{\mathrm{FE}}^{-1} [I_h^{1,1}(L_{\mathrm{ps}}\bar{x}^{(k)} - \bar{b}),\ J_h^{1,1}(\bar{\tilde{\sigma}}^{(k)} \cdot \bar{n} - \bar{g}_2)]. \tag{3.2}$$

The stability of this scheme using equal-order interpolants for velocities and

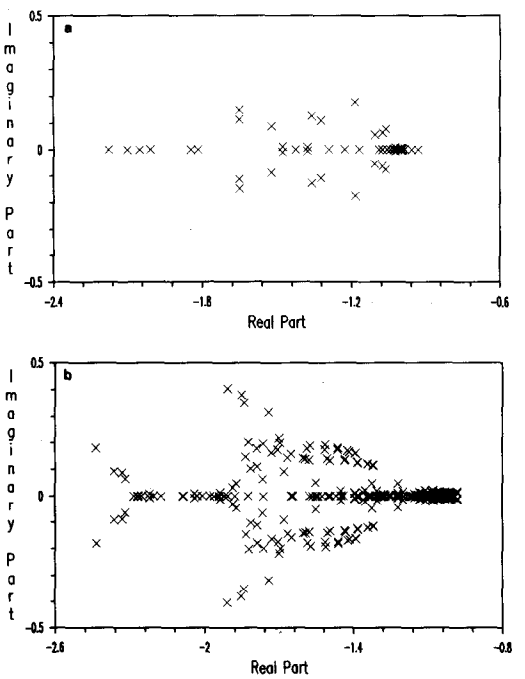

FIG. 2. Eigenvalue spectrum of A. Stokes problem preconditioned by $Q2$–$Q1$ FE. Natural boundary conditions: (a) $N=5$; (b) $N=13$.

TABLE III

Condition Number of A for the Stokes Problem Preconditioned by $Q2$–$Q1$ Element. Natural Boundary Conditions on sides $x = 1$ and $y = 1$.

N	$\lambda_{\max}$	$\lambda_{\min}$	$\frac{\lambda_{\max}}{\lambda_{\min}} = \kappa(A)$
5	2.177	0.9330	2.333
7	2.455	0.9664	2.540
9	2.470	0.9762	2.530
11	2.434	0.9787	2.487
13	2.442	0.9801	2.491
15	2.444	0.9810	2.491

pressure is achieved by adding a stabilization term in the discrete equations. The continuity equation in (2.28) is modified as

$$\sum_i h_i^2 \int_{R_i} \mathbf{grad}\, p_h \cdot \mathbf{grad}\, q_h \, dS + \int_\Omega q_h \operatorname{div} \bar{u}_h \, d\Omega = 0, \qquad R_i \in \mathscr{R}_N. \tag{3.3}$$

In (3.3), h_i^2 denotes some measure at the elemental level. This element does not require the inf-sup condition anymore. It seems to be a very attractive preconditioner as no spurious pressure mode has to be filtered. However, the eigenvalue analysis shows dismal performances. As Table IV exhibits, the maximum eigenvalue of A goes to 2 as for the $Q2$–$Q1$ preconditioner. In addition of the seven zero eigenvalue corresponding to the spectral spurious pressure modes, the minimum nonvanishing eigenvalue goes to zero when the discretization becomes finer. The iteration (3.2) cannot converge to the spectral solution within an adequate finite number of iterations. Figure 3 shows the spectrum of A which lies between 0 and

TABLE IV

Eigenvalue Analysis of A for the Preconditioned Stokes Problem by $Q1$–$Q1$ Finite Elements. Dirichlet Boundary Conditions

N	$\lambda_{\max}$	$\lambda_{\min}$
5	1.406	$3.465\ 10^{-3}$
7	1.610	$1.670\ 10^{-3}$
9	1.711	$8.523\ 10^{-4}$
11	1.773	$4.890\ 10^{-4}$
13	1.816	$3.053\ 10^{-4}$
15	1.853	$2.031\ 10^{-4}$

-2 for $N=13$. The bunch of eigenvalues in the interval $]-1, 0]$ corresponds to the stabilization term of (3.3). They accumulate near the origin with increasing values of N.

3.3. *The Q1–Q0 Element*

The pseudospectral iterates are computed by the relation

$$\bar{x}^{(k+1)} = \bar{x}^{(k)} - \alpha_k I_N L_{\mathrm{FE}}^{-1} [I_h^{1,0}(L_{\mathrm{ps}}\bar{x}^{(k)} - \bar{b}),\ J_h^{1,0}(\bar{\bar{\sigma}}^{(k)} \cdot \bar{n} - \bar{g}_2)], \tag{3.4}$$

where

$$I_N = \begin{Bmatrix} I_N^v \\ I_{N-1}^{q,0} \end{Bmatrix}.$$

In $\mathscr{R}_N$, pressures are attached to the nodes of $\mathbf{G}_{0,N}$. This pressure arrangement is coherent with the weak formulation (2.28). The analysis carried out by Sani *et al.* [20] shows the presence of two spurious modes: the hydrostatic and checkerboard (CB) modes. This last spurious mode is a numerical artifact triggered by the solution of the Stokes problem where two pressures are imposed at well-selected points in order to remove the singularity of the algebraic system.

On $\mathbf{G}_N$, the global CB mode is an odd function of the space variables and is known to within a multiplicative constant.

3.3.1. *FE Filter.* Denoting by $\bar{p}^e$ the CB mode at the element level, one knows that

$$\bar{p}^e = \pm k/A^e, \tag{3.5}$$

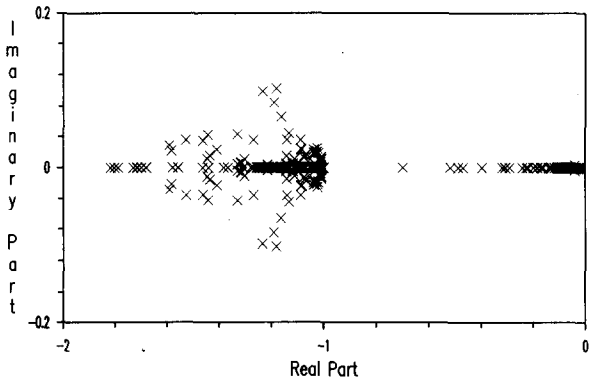

FIG. 3. Eigenvalue spectrum of A. Stokes problem preconditioned by $Q1$–$Q1$ FE. Dirichlet boundary conditions. $N=13$.

where A^e is the element area and k is an unknown constant. The filter proposed by Sani *et al.* [20] weighs the CB mode over four adjacent elements:

$$\sum_{i=1}^{4} \bar{p}^i A^i = 0. \tag{3.6}$$

The filtered pressure field is then computed on a smoothed grid such that

$$p'_j = \sum_{i=1}^{4} p^i A^i \Big/ \sum_{i=1}^{4} A^i, \tag{3.7}$$

where the coordinates of the new pressure node are defined by the following relations (depicted in Fig. 4):

$$x'_j = \sum_{i=1}^{4} x_i A^i \Big/ \sum_{i=1}^{4} A^i, \qquad y'_j = \sum_{i=1}^{4} x_i A^i \Big/ \sum_{i=1}^{4} A^i, \tag{3.8}$$

In the right-hand side of (3.7), the p^i are FE (polluted) pressures. The coordinates (3.8) are those of the centroid of each group of four neighbouring elements. Near the boundaries, one considers only groups of two elements. Corners are handled by a least squares solution or by linear interpolation. From the interior points of the smoothed mesh, one obtains the pressure in Chebyshev space through Chebyshev interpolation. The matrix of the interpolation problem is symmetric and diagonally dominant. It is solved by a Choleski decomposition. The pressures in spectral space are in $\mathbf{P}_{N-1}$. Let us notice that the filtering process (3.7)–(3.8) is only second-order accurate.

3.3.2. *Spectral filter.* Here, the Chebyshev representation interpolates pressure values which flipflop signs from one point to the next one in both directions. As these pressures are defined on $\mathbf{G}_{0,N}$, i.e., at the average values of the Chebyshev collocation points, we will now show that the zeroes of the CB mode are located on the grid $\mathbf{G}_{0,\mathrm{CB}}$ defined by (2.18). This will be done for 1D interpolation because the extension to an n-D case is straightforward by the tensor-product character of the approximation.

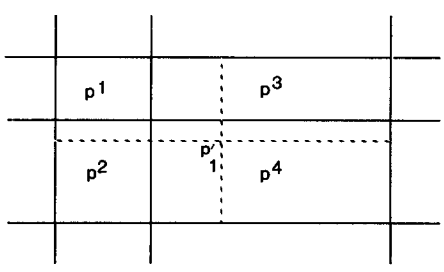

FIG. 4. FE polluted and filtered pressures on a patch of 4 elements.

Let us denote by m_k the points of $\mathbf{G}_{0,N}$. From the definition, we obtain

$$m_k = \frac{x_k + x_{k-1}}{2} = \cos\frac{\pi}{2N}\cos\frac{\pi(2k-1)}{2N} = \xi_k \cos\frac{\pi}{2N} = \xi_1 \xi_k, \tag{3.9}$$

where ξ_k are the zeroes of the polynomial T_N. The pressure is the Lagrange interpolant built on the N abcissae m_k and may be written as

$$p(x) = \sum_{k=1}^{N} p_k l_k(x), \tag{3.10}$$

with

$$\begin{aligned} l_k(x) &= \frac{\omega(x)}{(x-m_k)\,\omega'(m_k)}, \\ \omega(x) &= (x-m_1)(x-m_2)\cdots(x-m_N). \end{aligned} \tag{3.11}$$

As $\mathbf{G}_{0,N}$ is the array of the interpolation nodes, $\omega(x) = \xi_1^N T_N(x/\xi_1)$, and therefore

$$\begin{aligned} p(x) &= T_N\left(\frac{x}{\xi_1}\right) \sum_{k=1}^{N} \frac{p(m_k)\,\xi_1}{(x-m_k)\,T'_N(\xi_k)}, \\ &= \frac{T_N(x/\xi_1)}{N} \sum_{k=1}^{N} (-1)^{k-1} \frac{p(m_k)\,\xi_1 (1-\xi_k^2)^{1/2}}{(x-m_k)}, \\ &= \pm \frac{T_N(x/\xi_1)}{2N \sin \pi/2N} \sum_{k=1}^{N} \frac{1}{(x/\xi_1 - \xi_k)}. \end{aligned} \tag{3.12}$$

We have used (3.5) to get (3.12) with $A_k^e = \cos(\pi k/N) - \cos(\pi(k-1)/N)$. With the identity

$$T'_N\left(\frac{x}{\xi_1}\right) = \sum_{k=1}^{N} \frac{T_N(x/\xi_1)}{(x/\xi_1 - \xi_k)},$$

the right-hand side of Eq. (3.12) becomes

$$p(x) = \pm \frac{T'_N(x/\xi_1)}{2N \sin \pi/N}. \tag{3.13}$$

This expression vanishes for the values

$$\cos\frac{\pi}{2N}\cos\frac{\pi k}{N} = \frac{1}{2}\left(\cos\frac{2k-1}{N}\cdot\frac{\pi}{2} + \cos\frac{2k+1}{N}\cdot\frac{\pi}{2}\right),$$

which define the mesh $\mathbf{G}_{0,\mathrm{CB}}$.

The spectral filter works as follows. From the centered pressures on $\mathbf{G}_{0,N}$, a Chebyshev interpolation yields the unfiltered representation in Chebyshev space.

From this approximation, the pressure is evaluated on $\mathbf{G}_{0,\mathrm{CB}}$. Finally, a Chebyshev interpolation on $\mathbf{G}_{0,\mathrm{CB}}$ provides the final spectral pressures. They are in $\mathbf{P}_{N-2}$ as the pressures are the result of $R_{N-1} I_{N-1}^{q,0}$ (Eq. (2.17)).

It should be noticed that this filter yields pressures in $\mathbf{P}_{N-2}$. This is analogous to the new Legendre spectral element method [21], where a staggered mesh for the pressure is used with a classical Legendre grid for the velocity components.

3.3.3. *Poisson equation.* Finally, a third algorithm resorts to the solution of a Poisson equation for the pressure

$$\Delta p = S \qquad \text{in } \Omega, \tag{3.14}$$

with the boundary conditions

$$\frac{\partial p}{\partial n} = \mu \frac{\partial^2 u_n}{\partial n^2} \qquad \text{on } \partial\Omega. \tag{3.15}$$

In (3.15), $\partial p/\partial n$ denotes the normal derivative to the wall and u_n is the normal component of the velocity field. A fast Helmholtz spectral solver [5] is used for (3.14). The finite element code is only useful to obtain the velocity field. This third procedure is less general than the two previous ones because the Helmholtz solver is restricted to simple geometric configurations.

4. Numerical Results

Two numerical test problems were performed. The first one is an analytical Stokes problem where a smooth solution exists. The second one is the regularized square cavity problem [22].

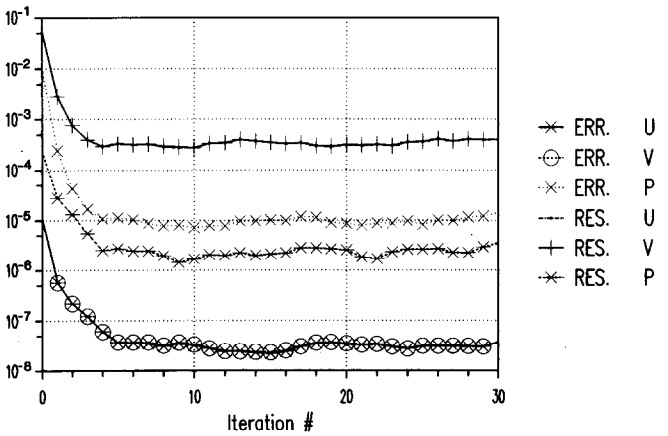

FIG. 5. Convergence history (errors and residuals) vs number of iterations. Theoretical solution: $a = \frac{1}{2}$, $N = 13$, $Q2$–$Q1$ FE, Dirichlet boundary conditions. Relaxation factor set to unity.

4.1. *Analytical Stokes Problem*

A full solution of the Stokes problem (2.1), (2.2) may be written in the general form:

$$u = -\cos a\pi x' \cdot \sin a\pi y', \tag{4.1}$$

$$v = \sin a\pi x' \cdot \cos a\pi y', \tag{4.2}$$

$$p = -2a\pi \sin a\pi x' \cdot \sin a\pi y', \tag{4.3}$$

$$f_x = 4a^2\pi^2 \cos a\pi x' \cdot \sin a\pi y', \tag{4.4}$$

$$f_y = 0. \tag{4.5}$$

In the previous relations, $x' = x + \delta x$, $y' = y + \delta y$ in such a way that a, δx, and δy are adjustable parameters to control the spatial behaviour of the solution. In the sequel, let us set $a = \frac{1}{2}$, $\delta x = \delta y = 0$, and $\bar{\Omega} = [0, 1]^2$. Errors on the velocity and pressure fields are computed in the L_∞ norm on $\mathbf{G}_N$, as well as the residue of each momentum equation and the continuity constraint.

4.1.1. *The Q2–Q1 element.* Figures 5, 6, and 7 show on 12×12 elements the convergence history versus the number of iterations, when Dirichlet boundary conditions are imposed. The α_k value in (3.1) is set to 1 in Fig. 5. One observes that the iterative procedure does not produce machine accuracy because the choice of α_k is not appropriate.

Figure 6 is obtained with $\alpha_k = \frac{1}{2}$. As the iterative process is now underrelaxed, spectral convergence is achieved in 30 iterations. Figure 7 corresponds to the optimal choice $\alpha_k = \frac{2}{3}$. Machine accuracy, for both u and v is attained in 21 iterations (bottom curve), while the pressure lags behind by four orders of magnitude. The residual on momentum equations (top curve) is worse than the residual on the

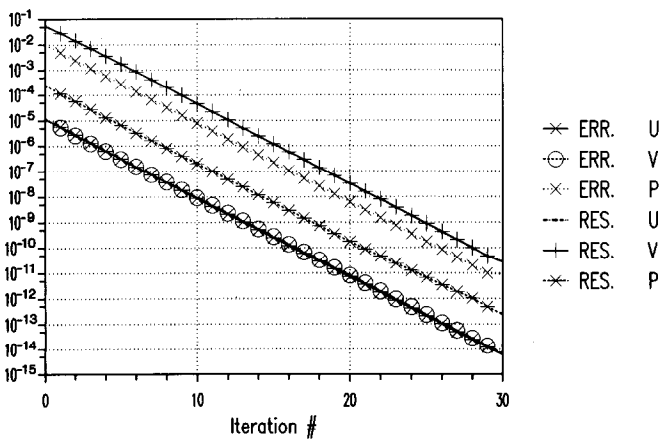

FIG. 6. Convergence history (errors and residuals) vs number of iterations. Theoretical solution: $a = \frac{1}{2}$, $N = 13$, $Q2$–$Q1$ FE, Dirichlet boundary conditions. Relaxation factor fixed to 0.5.

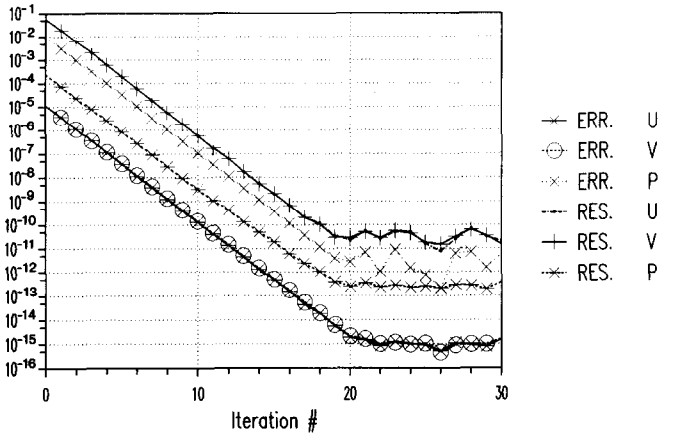

FIG. 7. Convergence history (errors and residuals) vs number of iterations. Theoretical solution: $a = \frac{1}{2}$, $N = 13$, $Q2$–$Q1$ FE, Dirichlet boundary conditions. Optimal relaxation factor is used.

continuity equation because of the presence of the pressure gradient term. In Figure 8, the Stokes problem is solved with natural boundary condition on sides $x = 1$ and $y = 1$. The general trend of the different curves is similar to the Dirichlet case. We should notice that this preconditioner gave no spectral spurious pressure modes in our computations. The pseudocollocation technique picks up the spurious pressure gradients at points where these gradients do not vanish. Therefore, the residual calculation enforces them to go to zero.

4.1.2. *The $Q1$–$Q1$ element.* The convergence history in Fig. 9 ($\alpha_k = 1$) confirms the result of the previous eigenvalue analysis. The error decay is extremely slow.

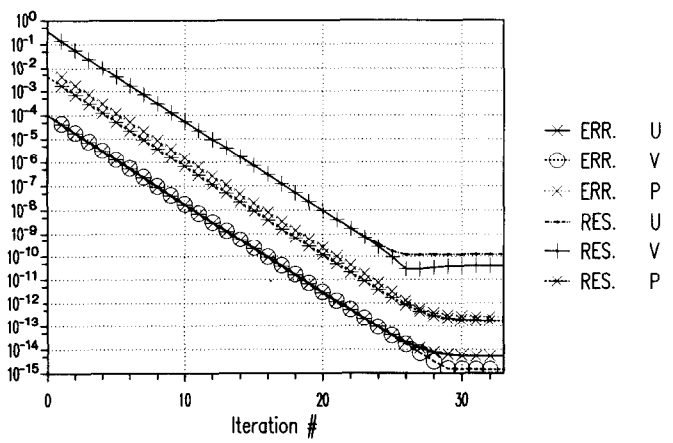

FIG. 8. Convergence history (errors and residuals) vs number of iterations. Theoretical solution: $a = \frac{1}{2}$, $N = 13$, $Q2$–$Q1$ FE, Natural boundary conditions. Optimal relaxation factor is used.

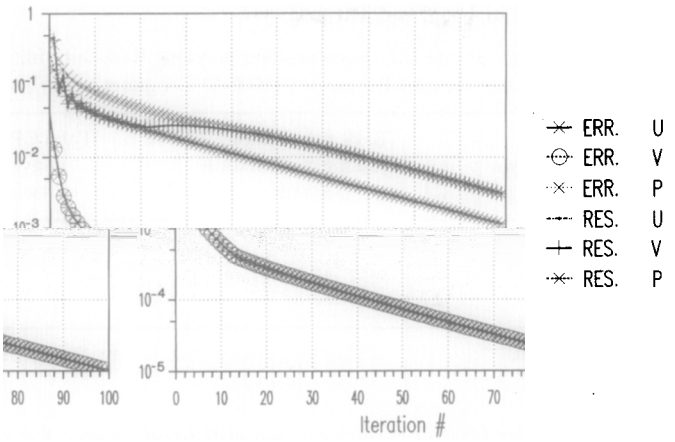

FIG. 9. Convergence history (errors and residuals) vs number of iterations. Theoretical solution: $a = \frac{1}{2}$, $N = 13$, $Q1$–$Q1$ FE, Dirichlet boundary conditions. Relaxation factor set to unity.

Despite the fact the computer time involved by each iteration is less than for the previous element, this poor behaviour stops this approach.

4.1.3. *The $Q1$–$Q0$ element.* For this element, the α_k parameter is not estimated through an eigenvalue study but comes from a dynamical calculation based on the error reduction process [5]. The final value of α_k is equal to 0.384.

Figure 10 displays the convergence histories which are of the same type as for the $Q2$–$Q1$ element, although the error decay is slower because of low-order Lagrangian interpolants.

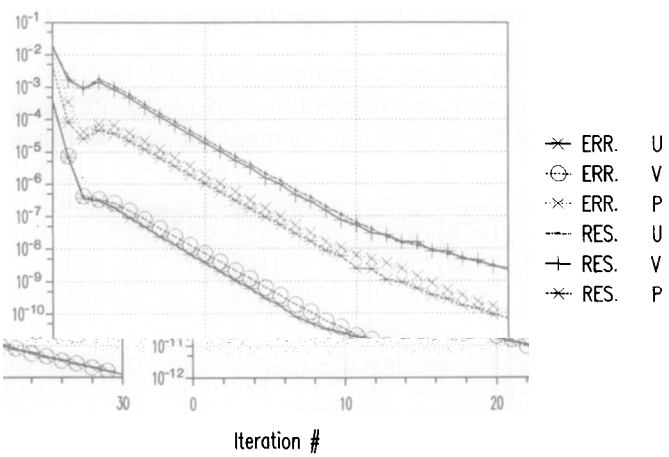

FIG. 10. Convergence history (errors and residuals) vs number of iterations. Theoretical solution: $a = \frac{1}{2}$, $N = 13$, $Q1$–$Q0$ FE, Dirichlet boundary conditions. Automatic relaxation is used.

TABLE V

CPU Time Required for one LU Decomposition and One Back-Substitution on a Data General Eclipse MV15000-20 Computer

Element	LU decomposition (seconds)	Back-substitution + residue computation (seconds)	Total CPU time for convergence[a] (seconds)
$Q2$–$Q1$	49	6.0	121
$Q1$–$Q0$	32	3.5	137
$Q1$–$Q1$	10	2.2	>230

[a] We defined the convergence by $|u_{\text{error}}| \leqslant 10^{-12}$.

To set up overall perspective for the final comparison, we still need an indication of the computational cost of each preconditioner. For that purpose, Table V gathers computer times for the LU decomposition and for the back-substitution with $N = 13$ for the three preconditioners.

To achieve an error of $O(10^{-12})$ on u, the $Q2$–$Q1$ preconditioner requires 12 iterations, while the $Q1$–$Q0$ performs 30 iterations. The amount of computing time is therefore very similar for both methods. However, we discarded the $Q1$–$Q0$ method because the presence of the CB mode implies a boundary constraint equation which may lead to a discrete ill-posed problem [20].

4.2. *The Regularized Square Cavity*

We quickly avoid the celebrated standard square cavity problem where upper corner singularities induce algebraic rates of convergence. The regularized square cavity [22] smoothes out the first-order singularities by imposing

$$u(x, 1) = 16x^2(x-1)^2, \qquad v(x, 1) = 0, \qquad x \in [0, 1],$$

and zero elsewhere for both velocity components ($\bar{\Omega} = [0, 1]^2$).

Figure 11 shows isobars and streamlines ($N_{x1} = N_{x2} = 13$. Plots use linear interpolants between nodes of $\mathbf{G}_N$). Table VI examines the rate of convergence of the

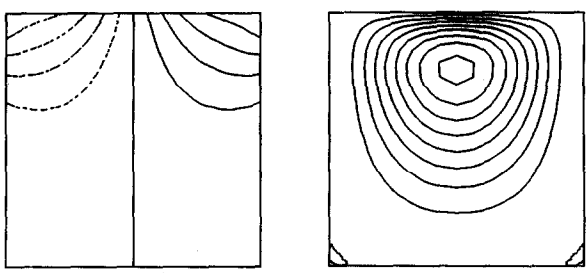

FIG. 11. Regularized square cavity problem, isobars, and streamlines, $N = 13$.

TABLE VI

Value of the u-Component of the Velocity at the Geometric Center of the Cavity with Respect to the Chebyshev Cutoff Value

N	$u(\frac{1}{2}, \frac{1}{2})$
5	−0.164578944706
7	−0.165408447324
9	−0.165468124154
13	−0.165473291361
17	−0.165473486334
21	−0.165473495005
25	−0.165473497888
33	−0.165473500662

Chebyshev approximation for the value of the u component at the geometric center of the cavity.

Let us denote $u(\frac{1}{2}, \frac{1}{2})$ by u_{mid}. If one takes the value of u_{mid} obtained with $N = 33$ as benchmark solution, one observes that the error decay is indeed spectral from $N = 5$ to 17, with $N = 9$ as an intermediate discretization.

Conclusions

This paper considered the problem of the Chebyshev pseudospectral approximation preconditioned by finite elements for the stationary Stokes equations. Three different elements were analyzed for the velocity–pressure formulation: the classical (9-nodes)$Q2$–$Q1$ Lagrangian element, the $Q1$–$Q1$ element proposed by Brezzi, and the $Q1$–$Q0$ element. An eigenvalue analysis of the preconditioned pseudospectral Stokes operator revealed that the $Q2$–$Q1$ element constitutes an interesting candidate for preconditioning. Numerical tests on analytical solutions and on the regularized square cavity problem were performed. It was observed that the theoretical analysis is corroborated. Therefore, the $Q2$–$Q1$ element is the best preconditioner even in the case where natural boundary conditions are applied. This result opens the way of multidomain decomposition [23, 24] which will be studied thoroughly in a further paper within the framework of the Navier–Stokes equations.

Acknowledgments

The authors are indebted to C. Canuto and A. Quarteroni for helpful discussions.

REFERENCES

1. D. GOTTLIEB AND S. A. ORSZAG, *Numerical Analysis of Spectral Methods: Theory and Applications*, SIAM monograph Vol. 26 (SIAM, Philadelphia, 1977).
2. M. DEVILLE, Recent developments of spectral and pseudospectral methods in fluid dynamics, VKI Lecture Series on Computational Fluid Dynamics, 1984.
3. S. A. ORSZAG, *J. Comput. Phys.* **37**, 70 (1980).
4. Y. MORCHOISNE, *Rech. Aérosp.* **5**, 293 (1979).
5. P. HALDENWANG, G. LABROSSE, S. ABBOUDI, AND M. DEVILLE, *J. Comput. Phys.* **55**, 115 (1984).
6. M. DEVILLE AND E. MUND, *J. Comput. Phys.* **60**, 517 (1985).
7. M. DEVILLE AND E. MUND, Finite element preconditioning for pseudospectral solutions of elliptic problems, *SIAM J. Sci. Stat. Comput.* (1989).
8. T. CARTAGE, P. DEMARET, AND M. DEVILLE, in *Proceedings 9th Int. Conf. Num. Methods. Fluid Dynamics*, edited by Soubbaramayer and J. P. Boujot, Lecture Notes in Physics Vol. 218, (Springer-Verlag, Berlin, 1985), p. 127.
9. C. CANUTO AND P. PIETRA, Istituto di Analisi Numerica del CNR, Pavia, Report n° 553, 1987 (unpublished).
10. P. CIARLET, *The Finite Element Method for Elliptic Problems* (North-Holland, Amsterdam, 1978).
11. M. DEVILLE AND G. LABROSSE, *J. Comput. Appl. Math.* **8**, 293 (1982).
12. D. ROSE, in *Graph Theory and Computing*, edited by R. Read (Academic Press, New York, 1973), p. 217.
13. A. GEORGE AND J. W. LIU, *SIAM J. Num. Anal.* **17**, 282 (1980).
14. F. BREZZI, *Rev. Fr. Automat. Rech. Oper. Sér. rouge*, Anal. Num. R–2, 129, (1974).
15. I. BABUSKA, *Num. Math.* **16**, 333 (1971).
16. F. BREZZI AND J. PITKARANTA, *Proceedings of a GAMM-Seminar* (Vieweg, Kiel, 1984). p. 11.
17. M. R. MALIK, T. A. ZANG, AND M. Y. HUSSAINI, *J. Comput. Phys.* **61**, 64 (1985).
18. Y. MORCHOISNE, "Résolution des équations de Navier–Stokes par une méthode spectrale de sous-domaines," 3° Conf. Internationale sur "Les méthodes numériques pour les Sciences de l'Ingénieur" (GAMNI), Paris, 1983.
19. C. BERNARDI, C. CANUTO, AND Y. MADAY, Generalized Inf.-Sup condition for Chebyshev approximation of the spectral Stokes problem, *SIAM J. Num. Anal.* **25**, 1237 (1988).
20. R. L. SANI, P. M. GRESHO, L. LEE, AND D. F. GRIFFITHS, *Int. J. Num. Fluids* **1**, 17 (1981).
21. Y. MAYDAY, A. T. PATERA, AND E. M. RØNQUIST, Optimal Legendre spectral element methods for the multi-dimensional Stokes problem, *SIAM J. Num. Anal.* (1989).
22. X. AUBERT AND M. O. DEVILLE, *J. Comput. Phys.* **49**, 490 (1983).
23. P. DEMARET AND M. O. DEVILLE, in *Computational Fluid Dynamics*, edited by G. de Vahl Davis and C. Fletcher (North-Holland, Amsterdam, 1988), p. 359.
24. P. DEMARET, M. O. DEVILLE, AND C. SCHNEIDESCH, Thermal convection solutions by Chebyshev pseudospectral multidomain decomposition and finite element preconditioning, *Appl. Num. Math.*, in press.